Atmos. Chem. Phys., 13, 4359–4372, 2013
www.atmos-chem-phys.net/13/4359/2013/
doi:10.5194/acp-13-4359-2013

Atmospheric Chemistry and Physics Open Access

Diurnal tracking of anthropogenic CO_2 emissions in the Los Angeles basin megacity during spring 2010

S. Newman[1], S. Jeong[2], M. L. Fischer[2], X. Xu[3], C. L. Haman[4], B. Lefer[4], S. Alvarez[4], B. Rappenglueck[4], E. A. Kort[5], A. E. Andrews[6], J. Peischl[7], K. R. Gurney[8], C. E. Miller[5], and Y. L. Yung[1]

[1]Division of Geological and Planetary Sciences, California Institute of Technology, Pasadena, CA 91125, USA
[2]Environmental Energy Technologies Division, E. O. Lawrence Berkeley National Laboratory, Berkeley, CA 94720, USA
[3]Department of Earth System Science, University of California, Irvine, CA 92697, USA
[4]Department of Earth and Atmospheric Sciences, University of Houston, Houston, Texas 77004, USA
[5]Earth Atmospheric Science, Jet Propulsion Laboratory, Pasadena, CA 91109, USA
[6]NOAA ESRL Global Monitoring Division, Boulder, CO 80305, USA
[7]NOAA ESRL Chemical Sciences Division, Boulder, CO 80305, USA
[8]School of Life Sciences, Arizona State University, Tempe, AZ 85287, USA

Correspondence to: S. Newman (sally@gps.caltech.edu)

Received: 20 January 2012 – Published in Atmos. Chem. Phys. Discuss.: 22 February 2012
Revised: 18 February 2013 – Accepted: 29 March 2013 – Published: 26 April 2013

Abstract. Attributing observed CO_2 variations to human or natural cause is critical to deducing and tracking emissions from observations. We have used in situ CO_2, CO, and planetary boundary layer height (PBLH) measurements recorded during the CalNex-LA (CARB et al., 2008) ground campaign of 15 May–15 June 2010, in Pasadena, CA, to deduce the diurnally varying anthropogenic component of observed CO_2 in the megacity of Los Angeles (LA). This affordable and simple technique, validated by carbon isotope observations and WRF-STILT (Weather Research and Forecasting model – Stochastic Time-Inverted Lagrangian Transport model) predictions, is shown to robustly attribute observed CO_2 variation to anthropogenic or biogenic origin over the entire diurnal cycle. During CalNex-LA, local fossil fuel combustion contributed up to $\sim 50\,\%$ of the observed CO_2 enhancement overnight, and $\sim 100\,\%$ of the enhancement near midday. This suggests that sufficiently accurate total column CO_2 observations recorded near midday, such as those from the GOSAT or OCO-2 satellites, can potentially be used to track anthropogenic emissions from the LA megacity.

1 Introduction

Climate change induced by increasing anthropogenic greenhouse gas emissions, especially CO_2, is a major societal issue today. It is important to understand the natural variability as well as emission sources from human activities in urban regions, which contribute disproportionately to the atmosphere's anthropogenic greenhouse gas burden (Gurney et al., 2009; Lee et al., 2006; Rayner et al., 2010). The large magnitude of emissions is easily detected by elevated concentrations in urban CO_2 domes (Idso et al., 1998; McKain et al., 2012; Pataki et al., 2003; Rice and Bostrom, 2010; Rigby et al., 2008; Kort et al., 2012) such as Los Angeles (LA), CA (Newman et al., 2008), and therefore makes megacities important sites for monitoring emissions reflecting rapidly changing natural and anthropogenic processes.

Here we use measurements of CO_2 and CO mixing ratios and planetary boundary layer height (PBLH) collected during the intensive CalNex-LA ground campaign of 15 May–15 June 2010, to demonstrate that ground-based measurements can be used to assess the magnitude and potential source of local CO_2 emissions in a megacity over the course of the entire diurnal cycle.

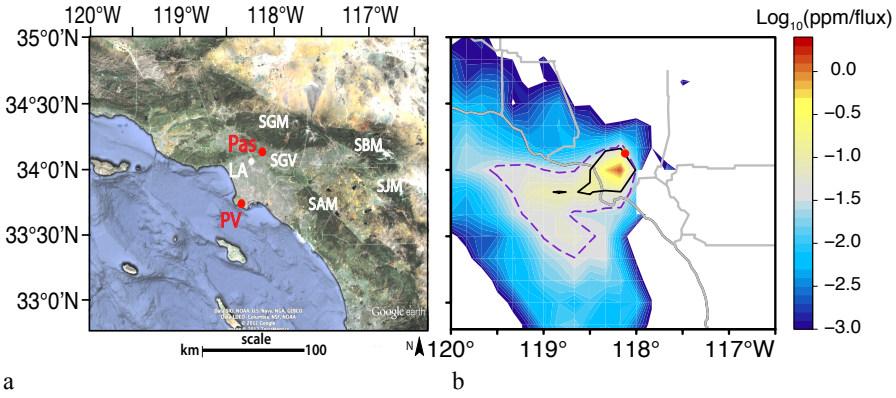

Fig. 1. (a) Google Earth map showing the location of Pasadena (Pas) in southern California. The sampling location was 34.14° N, 118.12° W, 246 m a.s.l.; the sampling height was 10 m above ground level. Also shown is the site on Palos Verdes Peninsula (PV) where CO_2 was measured for background air (see Appendix B1). Geographic features are indicated: LA – downtown Los Angeles; SGV – San Gabriel Valley; SGM – San Gabriel Mountains; SBM – San Bernardino Mountains; SJM – San Jacinto Mountains; SAM – Santa Ana Mountains. **(b)** Average midday footprint for the Caltech campus for 13:00 LT during the CalNex-LA campaign (see Appendix B3 for a description of the calculation). The color scale indicates the influence of different locations on the CO_2 measured in Pasadena, in ppm CO_2 in Pasadena/flux (flux in µmole s^{-1} m^{-2}) at the indicated location. Gray lines indicate county boundaries. The dashed purple contour surrounds the area that contributes 70 % of the surface influence on the air sampled at the Caltech site; the solid black contour indicates the region contributing 50 % of the surface influence. The shape of this contour reflects the average midday wind direction, from the SW (Fig. 3c). The air sampled in Pasadena comes predominantly from the ocean, adding emissions from the LA basin as it passes over, making Pasadena a good receptor site for the megacity.

Combustion of fossil fuels is the major local source of both CO and CO_2 in urban environments; however, the biosphere can introduce important sources and sinks for CO_2 (e.g., Pataki et al., 2003), resulting in differences in behavior for the two species. Both combustion and biological contributions are affected by transport of local and regional air masses to the sampling site and by dilution effects due to variations in PBLH. The latter is especially important when surface measurements are used to evaluate CO_2 mixing ratios for the total atmospheric column measured by satellite-borne instruments, which may be used to monitor CO_2 emissions worldwide. Indeed, Kort et al. have shown that persistent enhancements in the CO_2 urban domes over the Los Angeles and Mumbai megacities are observable by the Japanese Greenhouse Gas Observing Satellite (GOSAT) both in Mumbai, India, and in Los Angeles, during GOSAT's midday overpass (Kort et al., 2012). However, space-borne satellites in polar sun-synchronous orbits only observe at a fixed time of day, and they are not sensitive to the diurnal variations in urban emissions that may be critical for accurate validation of fuel-based inventory estimates or treaty verification.

2 Sampling location and methods

The CalNex-LA site, on the campus of the California Institute of Technology (Caltech) in Pasadena (Fig. 1a), is a good location for sampling LA basin emissions because long-lived components tend to be transported inland toward the San Gabriel Mountains, ∼4 km to the north, providing an integrated picture of daily emissions in the region. Air masses generally enter the region from the Pacific Ocean, 22 km to the southwest, and flow inland as the sun warms the land and the PBLH increases, exiting the region either through mountain passes or over the mountains if the PBLH increases sufficiently. The San Gabriel Mountains (1500–2000 m above sea level; a.s.l.) trap nighttime emissions in the basin during most nights, when temperature inversions put a shallow lid (< 100 m a.s.l.) on the mixed layer (Lu and Turco, 1994; Neiburger, 1969; Ulrickson and Mass, 1990).

Continuous in situ measurements of CO_2 and CO mixing ratios were collected from a 10 m tower near the NW corner of the Caltech campus. Ceilometer measurements of PBLH were made from the roof of a trailer about 10 m away from the in situ trace gas measurements. CO_2 mixing ratios were determined on a dried air stream using a G1101-i CO_2 Analyzer from Picarro Instruments (Sunnyvale, CA); CO was analyzed by vacuum ultraviolet (VUV) fluorescence using an AL5001 instrument from Aero-Laser GmbH (Garmisch-Partenkirchen, Germany). Planetary boundary layer height was measured by the minimum-gradient method using a Vaisala Ceilometer CL31 (Hamburg, Germany) to estimate the PBLH from aerosol backscatter profiles (Münkel et al., 2007). The 10 min averages for CO_2 and CO mixing ratios and 15 min averages for PBLH were combined into time series of hourly averages. Then campaign-wide averages for each hour were calculated to produce diurnal patterns.

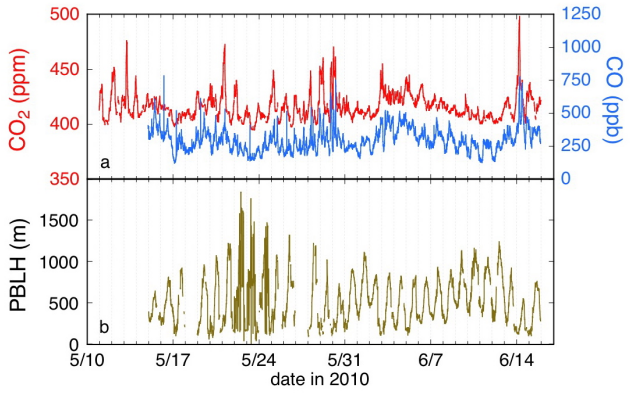

Fig. 2. Time series for the CalNex-LA period for **(a)** CO_2 and CO and **(b)** planetary boundary layer height (PBLH). Measurements plotted are 10 min averages for CO_2 and CO and 15 min averages for PBLH.

(Details regarding analytical methods and calculations are described in Appendices A and B.)

Background values for CO_2 mixing ratios were assumed to be constant for the duration of the campaign and were taken to be the average of the daily minimum hourly values at a site on Palos Verdes Peninsula overlooking the Pacific Ocean (393.1 ppm; Fig. 1a). This site is on a steep hillside $\sim$ 1.3 km from the ocean and $\sim$ 0.33 km a.s.l., with prevailing wind from the WSW. For CO, we used a time-varying background derived using NOAA Earth System Research Laboratory (ESRL) data from Pacific marine boundary layer and Pacific aircraft sites, as described in Appendix B1.

3 Results

Day-to-day variations of CO and CO_2 track each closely (Fig. 2a). For example, there is a peak on 2–3 June with gradually decreasing mixing ratios over the next eight days followed by an increase through the end of the campaign period, roughly inverse to the time series for PBLH (Fig. 2b). The time series for both CO and CO_2 show very low values overnight on 16–17 May and a long daytime minimum on 23 May (Fig. 2a). This minimum, which persists longer than any other daytime minimum, corresponds to the day with the strongest winds of the campaign, with hourly average winds up to 7 m s^{-1}, whereas the maximum average wind speed for all of the other days is 3 m s^{-1} (Fig. A3b).

Despite these similarities between the CO and CO_2 time series, there are significant differences in the averaged hourly diurnal patterns (Fig. 3a), even though both CO and CO_2 are long-lived atmospheric trace gases and might be expected to be affected similarly by changes in PBLH and advection. The major difference in their behaviors is the influence of the biosphere on CO_2 mixing ratios. Indeed, surface CO_2 concentrations increase at night and remain high until sunrise, probably due to respiration of the biosphere into the shallow nighttime stable layer, and then quickly drop as the boundary layer grows after sunrise, entraining air with lower CO_2. Photosynthesis during the day further depletes the boundary layer, with a minimum at $\sim$ 16:00 (all times in Pacific Standard Time). In contrast, there is a broad maximum in CO, from 08:00 to 17:00, centered at 12:00, probably due to transport of emissions from LA inland to Pasadena, as the daytime wind speed increases, bringing polluted air from morning "rush hour" in the basin to the sampling site (Figs. 1b, 3c). A second, smaller peak centered at $\sim$ 20:00 could reflect afternoon rush hour, on top of an increase in concentration due to development of a shallow temperature inversion layer (Fig. 3b), seen clearly in the diurnal CO_2 pattern. CO concentrations decline in the late evening after rush hour subsides, whereas CO_2 values remain high because of the persistent respiration source.

This late-spring CO_2 diurnal pattern exhibits $\sim$ 15 ppm variations compared to the $\sim$ 30 ppm variations observed for Vancouver, BC, Canada (Reid and Steyn, 1997), Phoenix, AZ (Idso et al., 2002), and Salt Lake City, UT (McKain et al., 2012). This may indicate that the San Gabriel Mountains are high enough to prevent complete venting of the LA megacity each day. In the other cities there is generally a small CO_2 peak in the morning associated with morning rush hour, whereas there is no morning peak in the Pasadena data. The Pasadena daily maximum occurs between 04:00 and 05:00, compared with 06:00–07:00 at approximately the same time of year in Phoenix and Salt Lake City. The record for Vancouver indicated no morning peak for June of 1993. In Phoenix, the summer diurnal pattern shows a broad afternoon (13:00–18:00) peak in CO_2 distinct from the evening increase (19:00–21:00) due to formation of the shallow inversion layer. Idso et al. (2002) interpret this peak as probably being due to transport of air from major freeways as wind speeds increase, similar to the Pasadena midday peak in CO. Data from neither Salt Lake City nor Vancouver show any evening rush hour peaks.

We use the diurnal patterns of CO and CO_2 in Pasadena to evaluate diurnal variations in the magnitude and source compositions of CO_2 in the Los Angeles basin.

4 Discussion

4.1 Effect of boundary layer thickness on surface signal

To first order, the top of the planetary boundary layer acts as an impenetrable barrier and prevents surface emissions from mixing with the atmosphere above. Trace gas concentrations within the PBL thus increase or decrease for a given emissions load as the PBL height falls or rises, respectively (Holzworth, 1967). This process is a major factor controlling the observed diurnal variations and potentially masks emissions' signals. Additionally, we must consider this diurnal

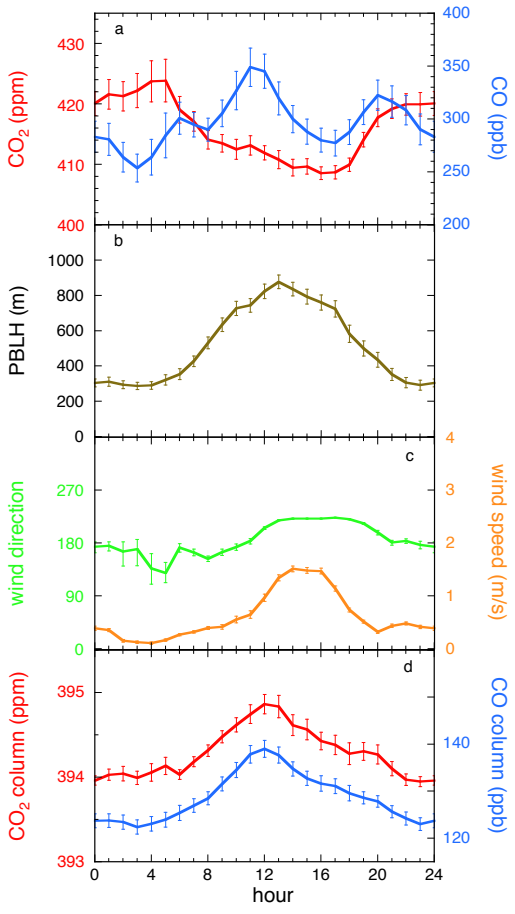

Fig. 3. Average diurnal patterns for **(a)** measured CO_2 and CO, **(b)** boundary layer height, **(c)** wind speed and direction for non-calm periods, and **(d)** CO_2 and CO in the atmospheric column, after correcting the measured values for changes in boundary layer height. Wind directions are plotted with north = 0° and 360°; east = 90°; south = 180°; and west = 270°. Error bars indicate standard deviations of the means ($n = 32$).

variation in PBLH when simulating the column mixing ratios observed by satellite-borne remote-sensing instruments. Reid and Steyn (1997) studied the effect of changing PBLH on CO_2 in Vancouver, BC, including lateral advection and entrainment. Advection is assumed to bring air masses containing emissions from the LA basin, based on the relatively local footprint of the site (Fig. 1b). In the simple box model described here, we ignore entrainment and look only at the simpler dilution effects, due to low wind speeds (Fig. 3c) and evidence from aircraft profiles (Fig. A1). We assume that it is the excess over the background mixing ratios (Fig. A2), not the underlying background, that is affected by changing boundary layer depth (Fig. 4a). As expected, the PBLH is greatest during midday (Fig. 3b), when warming inland air rises, increasing wind speed as air is drawn in from the ocean, and disrupts the shallow, stable inversion layer established overnight. We used PBLH measured by ceilometer to determine the mixed layer depth, as corroborated by profiles measured aboard the NOAA P3 aircraft (Fig. A1). In order to calculate the column mixing ratios from those measured on the surface, we must account for the changing size of the mixed layer. We determined the fraction of the atmosphere contained in the boundary layer (details in Appendix B2), which ranges from ∼0.03 overnight to ∼0.10 midday. The resulting contributions to the column CO_2 and CO are 0.8–1.8 ppm CO_2 and 4–21 ppb CO, from nighttime to midday. Although only a small fraction of the atmosphere is contained in the PBL, the magnitude of the emissions is large enough that variations within the PBL are discernable in total column observations. Indeed, they are large enough to be observable by satellites, such as the planned Orbiting Carbon Observatory 2 (OCO-2; Miller et al., 2007; Kort et al., 2012) observing during the early afternoon.

When these contributions are added to the background mixing ratios (393.1 ppm CO_2 and varying CO of ∼110–135 ppb; Fig. A2), the amplitude and timing of the diurnal patterns (Fig. 3d) for each component are consistent with column mixing ratios observed by an upward-pointing Fourier transform spectrometer (FTS) in spring of 2008 for the Pasadena area (at NASA's Jet Propulsion Laboratory (JPL), ∼5 km northwest of Caltech) by Wunch et al. (2011) (Fig. B1), supporting the assumptions that entrainment has negligible influence and that concentration variations both within and above the PBL are minor compared to the perturbation due to surface emissions. Although this pattern has indeed been previously observed (Wunch et al., 2011, 2009), this is the first instance of its report based on much less costly surface measurements. These diurnal patterns for the total atmospheric column (Fig. 3d) are significantly different from those measured at the surface (Fig. 3a) because there is a three-fold change in PBLH, which overwhelms the two-fold changes in the mixing ratio excesses above background. The broad midday peak for each species reflects anthropogenic emissions within the LA basin. No rush hour peaks are observed in the calculated column pattern.

4.2 Sources of local CO_2 emissions

CO is known to have virtually no natural sources in urban environments, but to result from incomplete combustion of fossil fuels (e.g., Chinkin et al., 2003), and therefore can be used to attribute CO_2 enhancements to fossil fuel combustion. Indeed, several studies (Gamnitzer et al., 2006; Levin et al., 2003; Turnbull et al., 2011, 2006; Vogel et al., 2010) have demonstrated that the ratio of the amounts of CO and CO_2 in excess of natural abundances (denoted as COxs and CO_2xs, respectively) can be used to determine the fraction of CO_2 derived from burning fossil fuels, denoted as F. This technique is not as successful as using radiocarbon to differentiate these sources, since it depends on assumptions as to the magnitude and variability of the emission ratio (F). On the other hand, the $\Delta^{14}CO_2$ method takes advantage of the

unambiguous fact that burning of fossil fuels produces CO_2 containing no ^{14}C. However, the CO/CO_2 technique is much more practical for use with continuous measurements than the more expensive and time-consuming $\Delta^{14}CO_2$ method (Vogel et al., 2010). A major assumption that must be made when determining F is the value of the CO/CO_2 emission ratio, denoted as R, here assumed to be constant over the time period of the campaign, although it probably does vary (Vogel et al., 2010). Djuricin et al. (2010) concluded that there is much uncertainty in R and therefore only very approximate values of F can be determined. They used R of 0.028 for data collected in Irvine, ~ 60 km SSE of Pasadena. Wunch et al. (2009) determined R in Pasadena to be 0.011 ± 0.002, using FTS, consistent with R from the California Air Resources Board for southern California (CARB, 2008) and significantly lower than that indicated by the EDGAR inventory (EDGAR, 2009). This value averages over the basin, including emissions from both petroleum and natural gas combustion sources, the latter of which should contribute negligible CO. It agrees with R calculated for the Sacramento area (Turnbull et al., 2011) using $\Delta^{14}CO_2$ and CO measurements.

Another possible complication to the use of CO/CO_2 ratios to determine anthropogenic emissions is the effect of fires. During the time period of this study, there was one fire, on 20–21 May 2010, in Home Gardens, CA, approximately 65 km ESE of the Caltech sampling site (http://cdfdata.fire.ca.gov/incidents/incidents_archived?archive_year=2010). However, we see no spike in CO or COxs / CO_2xs on this day (Figs. 2a and A3a), as would be expected if the site experienced contamination from the fire. In addition, during the time of the fire, the wind was never at a speed high enough from this direction for long enough to bring emissions from this combustion to the sampling site.

The time series of COxs / CO_2xs over the course of the CalNex-LA campaign (Fig. A3a) indicates a fairly constant, diurnally varying pattern for this ratio. This ratio does not reflect the diurnally varying PBLH, but rather the diurnally varying mix of fossil fuel and biogenic sources. COxs / CO_2xs ratios for the CalNex-LA data show a very distinctive diurnal variation (Fig. 4b), being lowest in the early morning (0.005) and highest in the early afternoon (0.012). We averaged the ratios for each hour to investigate the variation of F in Pasadena. Using R determined by Wunch et al. (2009) (0.011 ± 0.002), the resulting diurnal pattern (Fig. 4c) shows a maximum value for F within error of 1.0 during midday. The diurnal pattern for CO_2ff (Fig. 4d) directly reflects that for CO, since we are using a constant R. At night, this analysis suggests that 50 % of the local contribution is from anthropogenic combustion of fossil fuels. The other 50 % presumably comes from soil and plant respiration. The stable, shallow nighttime PBL (Fig. 3b) traps daytime emissions, so that F never falls much below 50 %, even though the dominant source (motor vehicle exhaust) decreases significantly during this time. The amount of CO_2 contributed by fossil fuels ranges from 12 to 21 ppm overnight to midday, respectively, and by the biosphere from uptake of ≤ 2 ppm during midday to a contribution of 17 ppm during early morning (Fig. 4d). One might presume that urban regions never experience significant biogenic CO_2 emissions. However, this nighttime result of ~ 50 % CO_2ff (Fig. 4c) is consistent with $\Delta^{14}CO_2$ results from February–March 2005 for Pasadena (Affek et al., 2007), for which 36 % of the local CO_2 contribution was attributed to biosphere respiration. During late spring, for the CalNex-LA campaign, it is reasonable to expect an even larger proportion of the nighttime emissions to be from respiration, since there is even more biomass during this late-spring time period. And significant respiration at night has been observed during spring and late summer/early fall in Salt Lake City, UT (Pataki et al., 2003). The observation that there is no significant biospheric component to local emissions during midday is probably due to a combination of the effects of the daytime anthropogenic emissions, the expanding boundary layer, and photosynthetic uptake of CO_2.

The validity of the major assumption of constant R needs to be evaluated, since it has implications for the importance of the biosphere in contributing CO_2 emissions in this urban environment. As a sensitivity test, we consider the case where F is constrained to be 1 throughout the diurnal cycle. In this case, R must vary from < 0.005 in the early morning hours to 0.012 during midday. A value as low as 0.005 has not been observed for urban regions (e.g., Bishop and Stedman, 2008). Since the unreasonably low value of R required to ensure no biogenic CO_2 input applies to the early hours of the morning (03:00–04:00), we conclude that at this time of day there must have been a significant contribution from the biosphere. Although we cannot provide a direct measure of R for this time period, we suggest that our assumed constant value of 0.011 ± 0.002 is reasonable, since it agrees with the lower limit in Heidelberg (Vogel et al., 2010) and the lowest value derived from the data of Bishop et al. (0.009; Bishop and Stedman, 2008).

Data from other methods are available to support the results from the CO/CO_2 data during midday. First, two measurements were made for $\Delta^{14}CO_2$ of CO_2 aggregated from flask samples collected at 14:00 on alternate days during 17–29 May (-6.4 ± 1.6 ‰) and 31 May–14 June (-20.6 ± 1.3 ‰) (Appendix A5). These $\Delta^{14}CO_2$ measurements indicate values for F of 0.9 ± 0.1–1.1 ± 0.1 (corresponding to 1.0 ± 0.1–1.1 ± 0.1 by the COxs / CO_2xs analysis for the same hours as the $\Delta^{14}CO_2$ samples) and 18 ± 3–24 ± 3 ppm CO_2 contributions (15 ± 3–17 ± 2 ppm for the COxs / CO_2xs analysis) for the average at 14:00 (Fig. 4d) in the early and late halves of the CalNex-LA period, respectively, consistent with the CO/CO_2 results. Second, the daytime result is also consistent with mass balance calculations of $\delta^{13}C$ and CO_2 for flasks collected at 14:00 during 2002–2003, which indicated that F of 0.71–1.0 could explain the observed stable isotopic composition (Newman et al., 2008). Third, the CO-based estimate of fossil fuel

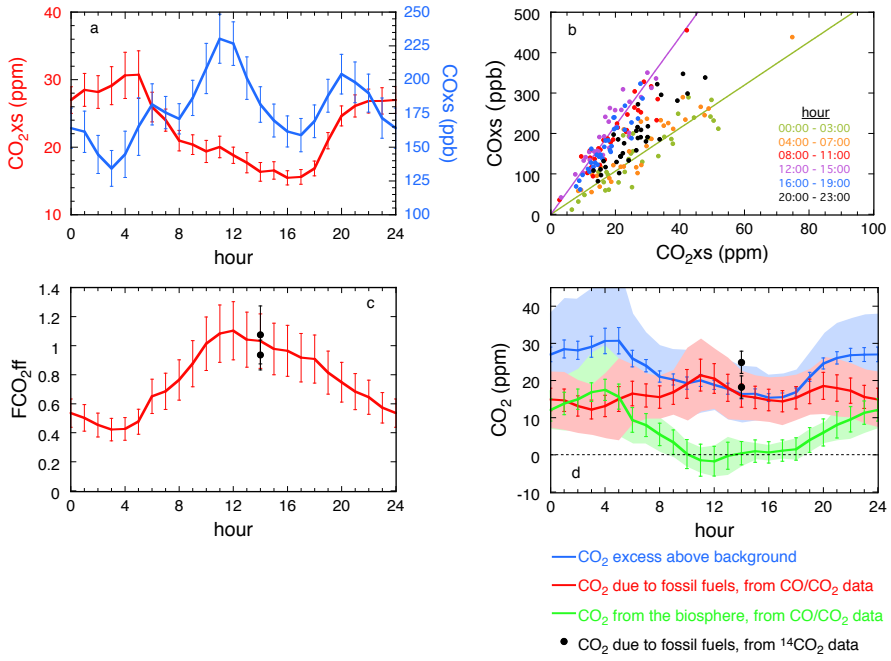

Fig. 4. (a) Excess (xs) CO_2 and CO over background levels (CO_2 background assumed to be constant at 393.1 ppm; CO background taken as time-varying, ranging from 96 to 136 ppb with an average of 115 ± 10 ppb; Appendix B1 and Novelli et al., 1991). **(b)** COxs vs. CO_2xs for hourly averages. Colors indicate time of day. Regression lines for early morning and early afternoon are shown in green and purple, respectively. **(c)** Diurnal variation of the fraction of fossil fuels (F) in the local contribution of CO_2 from CO / CO_2xs data shown in red. Black dots indicate data from $\Delta^{14}CO_2$. **(d)** Diurnal cycles for CO_2xs (blue), the amount of CO_2 emitted from fossil fuel combustion (CO_2ff; red), and the amount of CO_2 emitted from the biosphere (CO_2bio; green). Black dots indicate data for CO_2ff from $\Delta^{14}CO_2$. Calculations in **(c)** and **(d)** assume an emission ratio of CO / CO_2ff of 0.011 ± 0.002 from Wunch et al. (2009) and backgrounds for CO_2, CO, and $\Delta^{14}CO_2$ as described in Appendix B1. Error bars for F (**c**; red), CO_2ff (**d**; red), and CO_2bio (**d**; green) reflect the error in the emission ratio (18 % relative), for CO_2xs reflect standard errors ($n = 32$), and for CO_2ff from $\Delta^{14}CO_2$ reflect errors in measurements and backgrounds. Shaded regions in **(d)** indicate one standard deviation of the scatter in the hourly averages.

CO_2 agrees well (RMS difference ~ 5 ppm, 20 % compared to the 25 ppm range of measured and predicted CO_2ff enhancements from local emissions, very similar to the 18 % error on the CO / CO_2 results from the error on R) with predicted afternoon fossil fuel CO_2 signals calculated using WRF-STILT footprints combined with the Vulcan 2.0 fossil fuel inventory (see Appendix B4; Figs. B2 and B3). Figure B2 compares (1) the CO_2ff estimated using the continuous estimate of COxs measurements scaled to CO_2ff using the constant emission ratio, R, and (2) the CO_2ff estimated from WRF-STILT footprints convolved with the Vulcan 2.0 emission maps. The mean difference between the model predictions and measurements is a small and statistically insignificant offset of 2.6 ± 2.3 ppm as shown in Fig. B3, although residual errors in some combination of background, average footprint strength, and/or average emissions cannot be ruled out. Together, these different approaches confirm that high-precision measurements of CO and CO_2, combined with appropriate background measurements and determination of R, can give meaningful diurnal variation of local sources of fossil fuel CO_2.

As mentioned above, a wide range of values for R are given in the literature, including 0.009 (Bishop and Stedman, 2008) and 0.028 (Djuricin et al., 2010). However, the data from $\Delta^{14}C$ and $\delta^{13}C$ measurements preclude the use of R values toward the high end of the range given in the literature, such as the value of 0.028 used by Djuricin et al. (2010). This latter value leads to a maximum of ~ 40 % contribution from fossil fuels during midday, whereas the carbon isotopic data discussed above allow no less than 71 %. This lower limit for F during the CalNex-LA period constrains R to be ≤ 0.016.

We observe a single broad peak in CO_2 emissions during midday, unlike the pattern observed by McKain et al. (2012) for Salt Lake City, UT, who found two rush hour peaks during mornings and evenings. The single peak for Los Angeles is reasonable for this time of year and the low wind speeds we experience. Transport of the emissions from the heart of the basin during the morning takes some time to arrive at the receptor site in Pasadena. Indeed, downtown LA is 14 km away and therefore the peak should arrive about 4 h after emissions there, given an average wind speed of 1 m s^{-1}, and

the evening peak occurs ∼ 3–4 h after evening rush hour, at about 20:00. The lack of morning and evening local rush hour peaks probably reflects the fact that the boundary layer height is large during these times during summer. We do see morning local rush hour peaks during the winter, since rush hour begins before the boundary layer begins to expand, but it is frequently cut short by that expansion.

5 Conclusions

Attribution remains a central challenge to carbon cycle science. Here we have combined two known approaches, looking at CO / CO_2 ratios and using PBLH with a simple box model, and demonstrated a simple and affordable technique to diurnally differentiate anthropogenic and natural components of CO_2 observed in LA. CO_2 enhancements observed during May–June 2010 were composed of ∼ 100 % emissions from combustion of fossil fuels during the middle of the day, reducing to ∼ 50 % at night. These ratios were determined by diurnal variations of CO / CO_2 ratios and confirmed for 14:00 by $\Delta^{14}CO_2$. CO_2 from the biosphere varies dramatically, from contributing ∼ 17 ppm at 04:00 to uptake of ≤2 ppm at 11:00–12:00. Deployment of sensors to monitor CO_2, CO, and PBLH throughout a megacity such as LA would provide valuable attribution information to be used to determine trends of emissions as mitigation strategies are put into effect, especially if combined with radiocarbon measurements that provide an independent measure of R. Use of tracer ratios, such as $COxs / CO_2xs$, avoids some of the problems with assumptions that have to be made with modeling techniques. There are also implications of our results for remote sensing of CO_2 from space, as we confirm that midday column signals for Los Angeles can be attributed to anthropogenic activities and tracked over time. Our results are consistent with the previous observation of column CO_2 from a ground-based solar-viewing Fourier transform spectrometer (Wunch et al., 2009), and the signals are large enough to be detected by an OCO-like sensor (Miller et al., 2007). Kort et al. (2012) have shown clearly that the anthropogenic signal is visible from space, in this case using the Japanese Greenhouse Gas Observing Satellite (GOSAT). With time, accumulated data will demonstrate trends in this greenhouse gas over cities globally, and modeling, validated by observations, will be able to provide information on the emissions giving rise to these trends. However, well-studied regions using the techniques demonstrated here will be needed to validate the results from space-borne measurements and to extend the analysis to all hours of the day.

Appendix A

Analytical methods

A1 Site description

As with all cities, there are a few trees nearby and there are surface streets surrounding the block of the campaign site. The closest highway is ∼ 1 km to the north. Although the closest power plant, Caltech's cogeneration plant, is ∼ 1 km SW of the site, its combustion products cannot be producing the trends we observed, since its fuel consumption is constant over time.

A2 Analyses of CO_2 mixing ratios

We determined CO_2 mixing ratios by wavelength-scanned cavity ring-down spectroscopy using a G1101-i Isotopic CO_2 Analyzer from Picarro Instruments (Sunnyvale, CA). Air CO_2 values were measured after passing the sample stream through $Mg(ClO_4)_2$ to remove H_2O. The values reported are averages of consecutive 10 min periods of 5 min running averages of measurements taken every ∼ 8 s. The instrument was calibrated daily for CO_2 using three dry air standard tanks from NOAA, with each gas run for 30 min. The standards contained 378.87 ± 0.03, 415.15 ± 0.06, and 493.74 ± 0.03 ppm, respectively. The calibration line for each day was determined by regression of standard values determined by the average of 10 min of 5 min running averages after purging the instrument with each standard for 15 min. The average uncertainty for the CO_2 mixing ratio measurements was ±0.08 ppm. Because of the excellent temperature control within the optical cavity ($\pm 0.002\,^{\circ}C$; 1σ), there was no diurnal variation due to large diurnal temperature changes (on the order of $\pm 1.5\,^{\circ}C$; 1σ) observed in the portable trailer used as a laboratory for the field campaign.

We used data from a site on Palos Verdes Peninsula (33.74° N 118.35° W; 335 m a.s.l.) to determine CO_2 background mixing ratios for calculations described below. Data were collected every 20 s by a CIRAS-SC (PP Systems, Amesbury, MA) non-dispersive infrared gas analyzer after passing through $Mg(ClO_4)_2$ to dry the air stream. This instrument maintains stability by running a zero every 30 min. The span of the instrument was calibrated twice a week using a standard air tank from NOAA (420.18 ± 0.03 ppm). The average uncertainty was ± 0.5 ppm. The data from this site are shown in Fig. A2a.

A3 Analysis of CO mixing ratios

CO was analyzed by vacuum ultraviolet fluorescence using an AL5001 CO instrument from Aero-Laser GmbH (Garmisch-Partenkirchen, Germany). The analytical method is based on the fluorescence of CO at 150 nm (Gerbig et al., 1999). The sources of calibration uncertainty include the uncertainty of the NIST (National Institute of Standards and

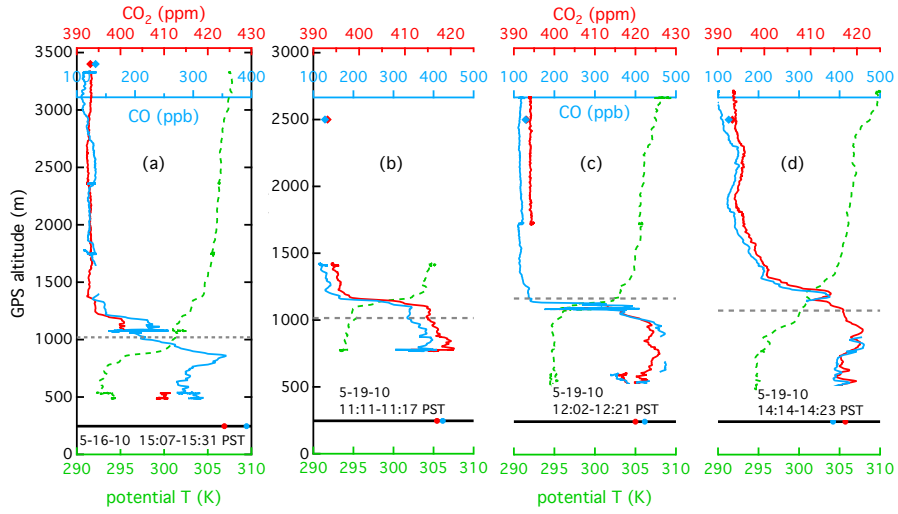

Fig. A1. Profiles of CO_2 (solid red curve) and CO (solid blue curve) mixing ratios and potential temperature (dashed green curve) determined by instruments on NOAA's P3 over the CalNex-LA ground site in Pasadena. Circles and diamonds show the compositions of CO_2 (red) and CO (blue) at the ground site and in the free troposphere, respectively, assumed to be the background values. The horizontal black lines indicate the elevation of the sampling site. The dashed gray lines indicate the location of the top of the mixed layer determined by the ceilometer at the ground site. These profiles show the rapid transition from PBL to free troposphere and the limited entrainment of PBL CO and CO_2 into the overlying atmosphere, at least for 19 May 2010. The maximum PBLH prior to the profile of 19 May 2010 at 14:00 was 1205 m, whereas the other profiles were collected at the time of the maximum PBLH. Unfortunately, the profiles determined later in the campaign did not extend low enough to intersect the PBL.

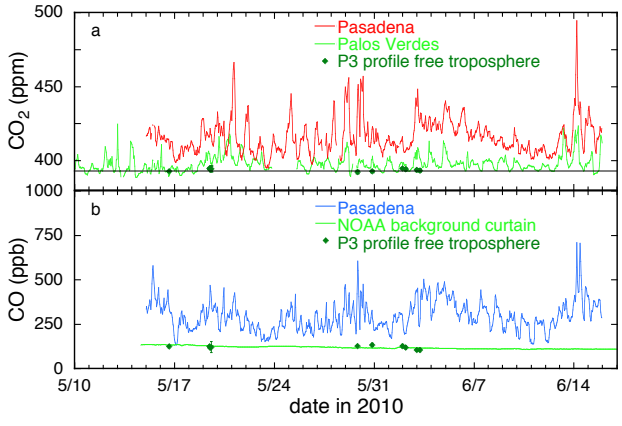

Fig. A2. (a) Time series for CO_2 for the period of the CalNex-LA campaign comparing measurements in Pasadena with those from Palos Verdes Peninsula, on a hillside overlooking the ocean. The average daily minimum CO_2 mixing ratio in Palos Verdes of 393.1 ppm, indicated by the horizontal black line, was used for the CO_2 background in all calculations. **(b)** Time series for CO in Pasadena compared with time-varying free-tropospheric CO from the NOAA Pacific boundary curtain, showing good agreement with P3 vertical profiles over the Pasadena site.

Technology) traceable calibration gas mixture (±2 %) from Scott Marrin, Inc. and the uncertainty of repeatability from the standard deviation of the slopes (±3.7 %) from twenty-nine daily calibrations. Temperature-sensitive parts of the CO instrument are maintained at 40 °C using a thermostat (Gerbig et al., 1999). Due to negligible temperature dependence, this type of instrument has been widely used in airborne missions and proved very reliable (e.g., Holloway et al., 2000). The combined uncertainty was estimated through propagation of the uncertainties as $((d_1)^2 + (d_2)^2 + (d_n)^2)^{1/2}$ with d_n defined as any individual uncertainty (e.g., calibration standard, repeatability, pressure, etc.) and was estimated ± 4.2 % (Taylor and Kuyatt, 1996). The detection limit was 9.8 ppbv (1σ) based on integration time of 10 s data. For CO, averages of 10 min of data collected every 10 s are presented in this paper.

A4 Planetary boundary layer height determination

Planetary boundary layer height was measured by the minimum-gradient method using a Vaisala Ceilometer CL31 (Hamburg, Germany) to determine aerosol backscatter profiles to estimate the PBLH (Münkel et al., 2007). This method assumes the aerosol gradient is a result of a temperature inversion associated with the entrainment zone, which marks the boundary between PBL and free-tropospheric air (Emeis and Schäfer, 2006; Schäfer et al., 2004). The reader is referred to Haman et al. (2012) for a detailed description of the instrument and settings used in this study. An overlap correction was not applied to the reported PBLH. The average uncertainty was ±5 m for the PBLH, and the lowest detectable PBLH of the ceilometer was 80 m due to height

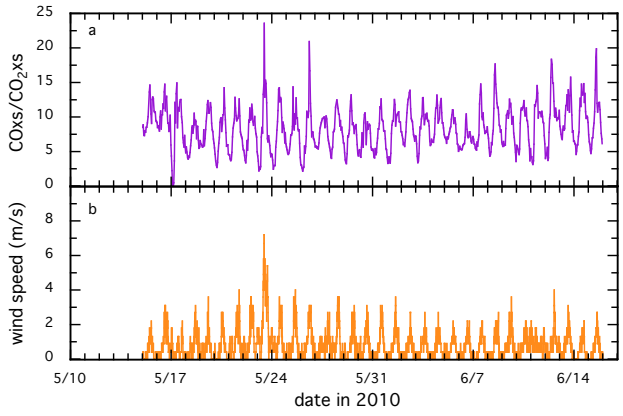

Fig. A3. Time series for **(a)** COxs / CO_2xs and **(b)** wind speed in Pasadena during the CalNex-LA campaign.

averaging constraints. Previous studies show overall agreement between ceilometer, radiosonde, and SODAR (sonic detection and ranging) estimated PBLHs during both stable and unstable conditions (e.g., Haman et al., 2012; Martucci et al., 2007; Münkel et al., 2007; van der Kamp and McKendry, 2010). Additionally, Haman et al. (2012) showed only a small bias (−23 m) between ceilometer and ozone profile estimates of the PBL height, which indicates collocation of the ozone- and aerosol-defined mixed layer height.

Four aircraft profiles were flown over the CalNex-LA ground site on 16 and 19 May 2010 (profiles a and c, respectively; Fig. A1), extending from the boundary layer into the free troposphere. Temperature and various chemical species, including CO and CO_2, were measured. Airborne CO measurements were provided by vacuum UV resonance fluorescence, with accuracy of ±5 % and precision of ±1 ppb (Holloway et al., 2000); airborne CO_2 measurements were provided by wavelength-scanned cavity ring-down spectroscopy (model 1301-m, Picarro Instruments, Sunnyvale, CA; Chen et al., 2010), with accuracy of ±0.10 ppm and accuracy of ±0.15 ppm.

A5 ^{14}C analysis

CO_2 was cryogenically extracted from air collected at 14:00 on alternate afternoons in evacuated 1 L Pyrex flasks (Newman et al., 2008). Two weeks' samples (7–8 flasks) were combined to produce two CO_2 samples for ^{14}C analysis, for the first and second halves of the CalNex-LA campaign (17–29 May and 31 May–14 June 2010). The CO_2 was graphitized using the sealed-tube zinc reduction method (Khosh et al., 2010; Xu et al., 2007). ^{14}C analysis was conducted at the Keck Carbon Cycle AMS facility at the University of California, Irvine (KCCAMS), where the system is a compact accelerator mass spectrometer (AMS) from National Electrostatics Corporation (NEC 0.5MV 1.5SDH-2 AMS system) with a modified NEC MC-SNIC ion source (Southon and Santos, 2004, 2007). The in situ simultaneous AMS δ^{13}C measurement at KCCAMS allowed for the correction of fractionation that occurred both during the graphitization process and inside the AMS system, and thus significantly improved the precision and accuracy of our measurements. The relative error of our day-to-day analysis, including extraction, graphitization and AMS measurement, is 2.5–3.1 ‰ based on our secondary standards processed during the past few years.

Appendix B

Data analysis calculations

B1 Averaging and backgrounds

Hourly averages were calculated for CO_2, CO, and PBLH measurements, respectively, through the time period of the CalNex-LA ground campaign. The diurnal patterns shown in Fig. 3 of the main text were produced by first generating hourly time series from the 10–15 min averages and then averaging the individual hours for all days of the campaign.

We determined the excess CO_2 and CO by subtracting the background concentrations for each component. We assumed that the background mixing ratios and isotopic values were constant for CO_2 and Δ^{14}C and time-varying for CO and reflected representative marine boundary layer values. For CO_2, we subtracted the average of the daily minima for Palos Verdes for the CalNex-LA time period (393.1 ppm; Fig. A2a), which is consistent with measurements for the free troposphere as measured by the NOAA P3 aircraft (Figs. A1 and A2a). We filter the CO_2 background data for boundary layer variations and local events by using the daily minimum values. For CO, suitable measurements of the background are not available, so we employed a method that has been used elsewhere for regional inverse modeling of CO_2 (e.g., Gourdji et al., 2012; Schuh et al., 2013) and N_2O (Jeong et al., 2012b). Briefly, discrete (i.e., flask) measurements of CO from sites in the NOAA cooperative air sampling network (Novelli and Masarie, 2012) are used to estimate time- and latitudinally varying CO values for the Pacific marine boundary layer. The methodology is identical to what is used to produce the GLOBALVIEW-CO (2012) product, but only Pacific sites operated by NOAA were included in the present study. Time- and latitude-dependent vertical gradients were estimated using CO data from Pacific and Gulf Coast sites in the NOAA Earth System Research Laboratory's aircraft network. The marine boundary layer and vertical profile information was combined into a time-, latitude- and altitude-dependent "curtain". The curtain is sampled at the western boundary of the modeling domain (130° W) for each of the 500 STILT trajectories corresponding to a particular observation, and the values are averaged, producing results that agree quite well with NOAA P3 CO observations during the CalNex-LA campaign (Fig. A2b). The CO background

mixing ratios varied from ∼135 ppb in the beginning of the time period to ∼112 ppb on 6 June, and ∼110 ppb at the end of the campaign. A similar time-varying background for CO_2 gives an average of 393.0 ± 1.1 ppm (1σ), which results in insignificant changes to diurnal hourly averages of CO_2xs relative to using the constant background. The diurnal patterns for the local contributions, in excess of the background values, are shown in Fig. 4a of the main text.

The background composition for $\Delta^{14}CO_2$ was taken to be 35.5 ± 2 ‰, derived from extrapolation of data for La Jolla to 31 May 2010, from the time series extending from 1 July 1992 to 7 December 2007 (Graven et al., 2012). This value was used in the calculation of the fraction of CO_2 added locally as fossil fuels, using Eq. (1) of Turnbull et al. (2011) and assuming no significant contribution from other sources such as biomass burning and heterotrophic respiration.

B2 Conversion of planetary boundary layer heights to pressure

For each hour of the campaign, the PBLH data were converted to pressure using a form of the hydrostatic equation assuming a constant lapse rate:

$$P = P_0 \cdot \left[1 - \frac{L \cdot h}{T_0}\right]^{\frac{-8}{L \cdot R}}, \quad \text{(B1)}$$

where P is pressure (Pa), P_0 is the standard pressure at sea level (101 325 Pa), L is the lapse rate near the surface (-0.0065 K m^{-1}), T_0 is the standard temperature of 288.15 K, R is the gas constant for air (287.053 J kg^{-1} K^{-1}), and h is altitude a.s.l. (m) (US Standard Atmosphere, 1976; Wallace and Hobbs, 1977). The fraction of the atmosphere contained in the boundary layer was calculated as the ratio of the difference between the pressures at the top and bottom of the boundary layer to the pressure at the surface $((P_{246\,\mathrm{m}} - P_{\mathrm{PBLH}})/P_{246\,\mathrm{m}}$; where $P_{246\,\mathrm{m}}$ is the pressure at the level of the in-situ surface measurements at 246 m a.s.l. and P_{PBLH} is the pressure at the top of the mixed layer). This fraction was multiplied by the surface mixing ratios of CO_2 and CO in excess of the background values to produce the amount of each component that was added to the total atmospheric column above Pasadena and then averaged for each hour of the day for weekdays and weekends, respectively. This approach assumes no entrainment during the diurnal cycle of increasing and decreasing PBLH. Indeed lack of significant entrainment is confirmed by aircraft profiles made over the sampling site during the campaign (Fig. A1), which show that the transition from the mixed layer to the overlying free troposphere is thin, less than 500 m thick for the four profiles showing it on 16 and 19 May 2010. The magnitude of variation of the diurnal patterns calculated here agree with those determined during May–June 2008 by Fourier transform spectroscopy (FTS) at NASA's Jet Propulsion Laboratory (JPL) ∼5 km to the NW of the CalNex-LA site (Fig. B1; Wunch et al., 2011). This agreement supports the adoption of these simplifying assumptions.

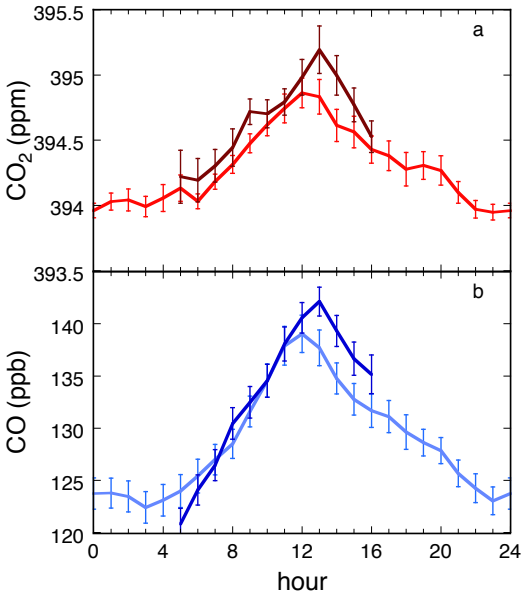

Fig. B1. Comparison of calculated column **(a)** CO_2 (red) and **(b)** CO (blue) mixing ratios at the CalNex-LA site on 15 May–15 June 2010 (lighter colors) with those measured on 1 May–22 June 2008 at JPL by FTS (darker colors), as part of the Total Carbon Column Observing Network (TCCON; Wunch et al., 2011; TCCON data (version GGG2012) were obtained from the TCCON Data Archive, operated by the California Institute of Technology, from the website at http://tccon.ipac.caltech.edu/). The TCCON mixing ratios were offset to match the CalNex-LA values (6 ppm CO_2 and 20 ppb CO added). Note that CO_2 mixing ratios vary ∼1 ppm and CO ∼15–20 ppb with peaks at 12:00 to 13:00 for both sets of measurements. The time period averaged for the TCCON data is longer than for the CalNex-LA data in order to have the same number of data points for the two data sets ($n = 32$, on average). Error bars indicate standard errors.

B3 Footprint calculations

The footprint (sensitivity of observation to surface emissions) was estimated using the Stochastic Time-Inverted Lagrangian Transport model (STILT; Lin et al., 2003), driven by meteorological fields generated by the Weather Research and Forecasting model (WRF; Nehrkorn et al., 2010). For the initial STILT calculations to determine the time-averaged footprint (Fig. 1b), 100 particles are released from the observation site at 13:00 local time for 15 May–15 June 2010, resulting in an error of 13 % (Gerbig et al., 2003). These particles are tracked as they move backward in time for 24 h, stochastically sampling the turbulence, and the footprint can be calculated from the particle density and residence time in the layer which sees surface emissions, defined as 0.5 PBLH (see citations for more details on STILT and STILT-WRF). The meteorological observations used to create the WRF wind

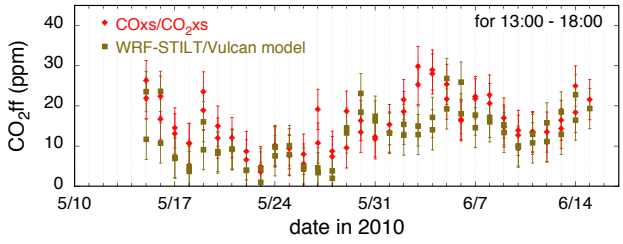

Fig. B2. Comparison of time series for CO_2ff determined using COxs / CO_2xs and constant R of 0.011 with that predicted using WRF-STILT and Vulcan 2.0 emissions, for 13:00–18:00, during the CalNex-LA campaign. For each day, average values are plotted for 13:00–15:00 and 16:00–18:00 for CO_2ff from both measurements and prediction. Error bars are ± 5 ppm, based on requiring that reduced $\chi^2 = 1$ during the linear regression calculation.

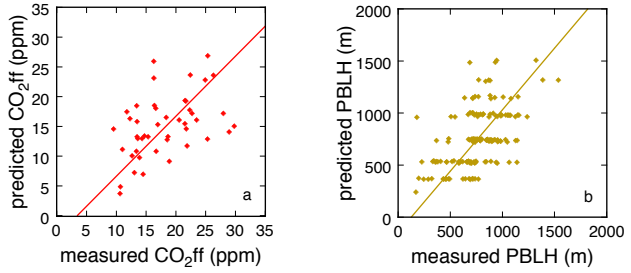

Fig. B3. Direct comparison of predicted versus measured **(a)** CO_2ff and **(b)** PBLH, for 13:00–18:00. The regression curves, based on requiring that reduced $\chi^2 = 1$, are as follows: CO_2ff predicted = −3.49 (± 3.21) + CO_2ff measured · 1.01 (± 0.19); RMSerror = 5 ppm; PBLH predicted = −147 (±78) + PBLH measured · 1.18 (± 0.10); RMSerror = 246 m.

fields for the footprint in Fig. 1b were initialized/nudged with Global Forecasting System (GFS; NOAA) winds and compared with a number of observations (Angevine et al., 2012). Footprint findings demonstrate the Caltech site is well situated for sampling the emissions signal from the LA basin. Based on this observation, we conclude that the effective sampling region in this time frame comprises the LA basin.

B4 Prediction of atmospheric fossil fuel signals

Predicted fossil fuel CO_2 (CO_2ff) mixing ratio signals were calculated using spatially and temporally resolved a priori CO_2ff emissions and WRF-STILT footprints using 5-day back trajectories. Comparisons between model results and measurements for CO_2ff are shown in Figs. B2 and B3a and for PBLH in Fig. B3b. The WRF runs follow methods applied by Zhao et al. (2009) for California methane, with modifications that included use of the Mellor–Yamada–Janjic (MYJ) boundary layer scheme (Janjic, 1990; Mellor and Yamada, 1982), nested sub-domains using spatial resolutions of 36 km, 12 km, and 4 km with 50 vertical layers, and two-way nesting from each outer sub-region. Following methods described in Jeong et al. (2012a), we compared WRF-simulated winds (modeled at a resolution of 4 km) with data from NOAA 915 MHz radar wind profiler (ftp://ftp1.esrl.noaa.gov/psd2/data/realtime/Radar915/) located at the Los Angeles Airport (LAX; lat = 33.94, lon = −118.44), the closest wind profiler to the GHG measurement site. Comparing WRF and profiler winds at a height of 182 m a.g.l. (the lowest available profiler level) for observation hours (13:00–18:00 local time), and removing (> 3 sd) outliers, the mean difference (1.1 ± 0.7 m s^{-1}, 95 % C.I.) is consistent with the expected (1 m s^{-1}) measurement accuracy of the profiler (Coulter, 2005), the best-fit slope (1.1 ± 0.2) from a reduced chi-square fit is consistent with unity (Press et al., 1992), and the RMS difference (2.1 m s^{-1}) is consistent with results for previous similar comparisons reported in Jeong et al. (2012a). Predicted boundary layer depths were compared with the ceilometer measurements (Fig. B3b). STILT footprints were calculated using 500 particles. Fossil fuel CO_2 emissions were obtained at hourly temporal and 10 km spatial resolution from the VULCAN2.0 inventory (http://vulcan.project.asu.edu/index.php).

Acknowledgements. We appreciate productive discussions with Paul Wennberg, Debra Wunch, Michael Line, Xi Zhang, Run-Lie Shia, and Joshua Kammer. WRF winds for the time-averaged footprints during the CalNex period were provided by Wayne Angevine of NOAA (Earth System Research Laboratory; ESRL). We thank Paul Novelli and Colm Sweeney of NOAA-ESRL for sharing their data that went into the NOAA background curtain product from which we calculated the time-varying background for CO. John S. Holloway (NOAA ESRL) provided the measurements of CO from the P3 aircraft profiles. As part of the CalNex-LA campaign, we gratefully acknowledge the support of Caltech and the California Air Resources Board in making the campaign successful. TCCON data (version GGG2012) were obtained from the TCCON Data Archive, operated by the California Institute of Technology, from the website at http://tccon.ipac.caltech.edu/. SN acknowledges financial support from JPL's Director's Research and Development Fund. Analysis by MLF and SJ was supported by the Director, Office of Science, of the US Department of Energy under Contract No. DE-AC02-05CH11231. We acknowledge the Keck Institute for Space Studies for financial support of publication costs and contribution by EAK.

Edited by: M. K. Dubey

References

Affek, H., Xu, X., and Eiler, J.: Seasonal and diurnal variations of $^{13}C^{18}O^{16}O$ in air: Initial observations from Pasadena, CA, Geochim. Cosmochim. Ac., 71, 5033–5043, 2007.

Angevine, W., Eddington, L., Durkee, K., Fairall, C., Bianco, L., and Brioude, J.: Meteorological model evaluation for CalNex 2010. Mon. Weather Rev., 140, 3885–3906, doi:10.1175/MWR-D-12-00042.1, 2012.

Bishop, G. A. and Stedman, D. H.: A decade of on-road emissions measurements, Environ. Sci. Technol., 42, 1651–1656, doi:10.1021/es702413b, 2008.

California Air Resources Board (CARB): California emission inventory data almanac, technical report, available from: http://www.arb.ca.gov/app/emsinv/emssumcat.php, 2008.

California Air Resources Board (CARB), National Oceanic and Atmospheric Administration (NOAA) and California Energy Commission (CEC): CalNex White Paper: Research at the Nexus of Air Quality and Climate Change, 1–12, available from: http://www.arb.ca.gov/research/fieldstudy2010/calnexus_white_paper_01_09.pdf, 2008.

Chen, H., Winderlich, J., Gerbig, C., Hoefer, A., Rella, C. W., Crosson, E. R., Van Pelt, A. D., Steinbach, J., Kolle, O., Beck, V., Daube, B. C., Gottlieb, E. W., Chow, V. Y., Santoni, G. W., and Wofsy, S. C.: High-accuracy continuous airborne measurements of greenhouse gases (CO_2 and CH_4) using the cavity ring-down spectroscopy (CRDS) technique, Atmos. Meas. Tech., 3, 375–386, doi:10.5194/amt-3-375-2010, 2010.

Chinkin, L., Coe, D., Funk, T., Hafner, H., Roberts, P., Ryan, P., and Lawson, D.: Weekday versus weekend activity patterns for ozone precursor emissions in California's South Coast Air Basin, J. Air Waste Manage. Assoc., 53, 829–843, 2003.

Coulter, R.: Radar Wind Profiler and RASS (RWP915) Handbook, ARM TR-044, 2005.

Djuricin, S., Pataki, D. E., and Xu, X.: A comparison of tracer methods for quantifying CO_2 sources in an urban region, J. Geophys. Res.-Atmos., 115, D11303, doi:10.1029/2009JD012236, 2010.

EDGAR Project Team: Emission database for global atmospheric research (EDGAR), release version 4.0., http://edgar.jrc.ec.europa.eu/index.php, Eur. Comm. Joint Res. Cent., Brussels, 2009.

Emeis, S. and Schäfer, K.: Remote sensing methods to investigate boundary-layer structures relevant to air pollution in cities, Bound.-Lay. Meteorol., 121, 377–385, doi:10.1007/s10546-006-9068-2, 2006.

Gamnitzer, U., Karstens, U., Kromer, B., Neubert, R. E. M., Meijer, H. A. J., Schroeder, H., and Levin, I.: Carbon monoxide: A quantitative tracer for fossil fuel CO_2?, J. Geophys. Res.-Atmos., 111, D22302, doi:10.1029/2005JD006966, 2006.

Gerbig, C., Schmitgen, S., Kley, D., Volz-Thomas, A., Dewey, K., and Haaks, D.: An improved fast-response vacuum-UV resonance fluorescence CO instrument, J. Geophys. Res.-Atmos., 104, 1699–1704, 1999.

Gerbig, C., Lin, J. C., Wofsy, S. C., Daube, B. C., Andrews, A. E., Stephens, B. B., Bakwin, P. S., and Grainger, C. A.: Toward constraining regional-scale fluxes of CO_2 with atmospheric observations over a continent: 2. Analysis of COBRA data using a receptor-oriented framework, J. Geophys. Res, 108, 4757, doi:10.1029/2003JD003770, 2003.

GLOBALVIEW-CO: Cooperative Atmospheric Data Integration Project – Carbon Monoxide. CD-ROM, NOAA ESRL, Boulder, Colorado [Also available on Internet via anonymous FTP to ftp.cmdl.noaa.gov, Path: ccg/co/GLOBALVIEW], 2012.

Gourdji, S. M., Mueller, K. L., Yadav, V., Huntzinger, D. N., Andrews, A. E., Trudeau, M., Petron, G., Nehrkorn, T., Eluszkiewicz, J., Henderson, J., Wen, D., Lin, J., Fischer, M., Sweeney, C., and Michalak, A. M.: North American CO_2 exchange: inter-comparison of modeled estimates with results from a fine-scale atmospheric inversion, Biogeosciences, 9, 457–475, doi:10.5194/bg-9-457-2012, 2012.

Graven, H. D., Guilderson, T. P., and Keeling, R. F.: Observations of radiocarbon in CO_2 at La Jolla, California, USA 1992–2007: Analysis of the long-term trend, J. Geophys. Res.-Atmos., 117, D02302, doi:10.1029/2011JD016533, 2012.

Gurney, K., Mendoza, D., Zhou, Y., Fischer, M., Miller, C., Geethakumar S., and du Can, S.: High Resolution Fossil Fuel Combustion CO_2 Emission Fluxes for the United States, Environ. Sci. Technol., 43, 5535–5541, 2009.

Haman, C. L., Lefer, B. L., and Morris, G. A.: Seasonal variability in the diurnal evolution of the boundary layer in a near coastal urban environment, J. Atmos. Ocean. Technol., 29, 697–710, doi:10.1175/JTECH-D-11-00114.1, 2012.

Holloway, J., Jakoubek, R., Parrish, D., Gerbig, C., Volz-Thomas, A., Schmitgen, S., Fried, A., Wert, B., Henry, B., and Drummond, J.: Airborne intercomparison of vacuum ultraviolet fluorescence and tunable diode laser absorption measurements of tropospheric carbon monoxide, J. Geophys. Res.-Atmos., 105, 24251–24261, 2000.

Holzworth, G. C.: Mixing depths, wind speeds and air pollution potential for selected locations in the United States, J. Appl. Meteorol., 6, 1039–1044, 1967.

Idso, C., Idso, S., and Balling, R.: The urban CO_2 dome of Phoenix, Arizona, Phys. Geogr., 19, 95–108, 1998.

Idso, S., Idso, C., and Balling, R.: Seasonal and diurnal variations of near-surface atmospheric CO_2 concentration within a residential sector of the urban CO_2 dome of Phoenix, AZ, USA, Atmos. Environ., 36, 1655–1660, 2002.

Janjic, Z.: The Step-Mountain Coordinate - Physical Package, Mon. Weather Rev., 118, 1429–1443, 1990.

Jeong, S., Zhao, C., Andrews, A. E., Bianco, L., Wilczak, J. M., and Fischer, M. L.: Seasonal variation of CH_4 emissions from central California, J. Geophys. Res, 117, D11306, doi:10.1029/2011JD016896, 2012a.

Jeong, S., Zhao, C., Andrews, A. E., Dlugokencky, E. J., Sweeney, C., Bianco, L., Wilczak, J. M., and Fischer, M. L.: Seasonal variations in N_2O emissions from central California, Geophys. Res. Lett., 39, L16805, doi:10.1029/2012GL052307, 2012b.

Khosh, M. S., Xu, X., and Trumbore, S. E.: Small-mass graphite preparation by sealed tube zinc reduction method for AMS C-14 measurements, Nucl. Instrum. Meth. B, 268, 927–930, 2010.

Kort, E. A., Frankenberg, C., Miller, C. E., and Oda, T.: Space-based observations of megacity carbon dioxide, Geophys. Res. Lett., 39, L17806, doi:10.1029/2012GL052738, 2012.

Lee, B. H., Munger, J. W., Wofsy, S. C., and Goldstein, A. H.: Anthropogenic emissions of nonmethane hydrocarbons in the northeastern United States: Measured seasonal variations from 1992-1996 and 1999-2001, J. Geophys. Res.-Atmos., 111, D20307, doi:10.1029/2005JD006172, 2006.

Levin, I., Kromer, B., Schmidt, M., and Sartorius, H.: A novel approach for independent budgeting of fossil fuel CO_2 over Europe by $^{14}CO_2$ observations, Geophys. Res. Lett., 30, 2194, doi:10.1029/2003GL018477, 2003.

Lin, J., Gerbig, C., Wofsy, S., Andrews, A., Daube, B., Davis, K., and Grainger, C. A.: A near-field tool for simulating the upstream influence of atmospheric observations: The Stochastic Time-Inverted Lagrangian Transport (STILT) model, J. Geophys. Res.-Atmos., 108, 4493, doi:10.1029/2002JD003161, 2003.

Lu, R. and Turco, R.: Air pollutant transport in a coastal environment. Part I: Two-dimensional simulations of sea-breeze and mountain effects, J. Atmos. Sci., 51, 2285–2308, 1994.

Martucci, G., Matthey, R., Mitev, V., and Richner, H.: Comparison between backscatter lidar and radiosonde measurements of the diurnal and nocturnal stratification in the lower troposphere, J. Atmos. Ocean. Technol., 24, 1231–1244, doi:10.1175/JTECH2036.1, 2007.

McKain, K., Wofsy, S. C., Nehrkorn, T., Eluszkiewicz, J., Ehleringer, J. R., and Stephens, B. B.: Assessment of ground-based atmospheric observations for verification of greenhouse gas emissions from an urban region, P. Natl. Acad. Sci. USA, 109, 8423–8428, doi:10.1073/pnas.1116645109, 2012.

Mellor, G. L. and Yamada, T.: Development of a turbulence closure model for geophysical fluid problems, Rev. Geophys. Space Phys., 20, 851–875, 1982.

Miller, C. E., Crisp, D., DeCola, P. L., Olsen, S. C., Randerson, J. T., Michalak, A. M., Alkhaled, A., Rayner, P., Jacob, D. J., Suntharalingam, P., Jones, D. B. A., Denning, A. S., Nicholls, M. E., Doney, S. C., Pawson, S., Boesch, H., Connor, B. J., Fung, I. Y., O'Brien D., Salawitch, R. J., Sander, S. P., Sen, B., Tans, P., Toon, G. C., Wennberg, P. O., Wofsy, S. C., Yung, Y. L., and Law, R. M.: Precision requirements for space-based X-CO_2 data, J. Geophys. Res.-Atmos., 112, D10314, doi:10.1029/2006JD007659, 2007.

Münkel, C., Eresmaa, N., Räsänen, J., and Karppinen, A.: Retrieval of mixing height and dust concentration with lidar ceilometer, Bound.-Lay. Meteorol., 124, 117–128, doi:10.1007/s10546-006-9103-3, 2007.

Nehrkorn, T., Eluszkiewicz, J., Wofsy, S. C., Lin, J. C., Gerbig, C., Longo, M., and Freitas, S.: Coupled weather research and forecasting-stochastic time-inverted lagrangian transport (WRF-STILT) model, Meteorol. Atmos. Phys., 107, 51–64, doi:10.1007/s00703-010-0068-x, 2010.

Neiburger, M.: The role of meteorology in the study and control of air pollution, B. Am. Meteorol. Soc., 50, 957–965, 1969.

Newman, S., Xu, X., Affek, H. P., Stolper, E., and Epstein, S.: Changes in mixing ratio and isotopic composition of CO_2 in urban air from the Los Angeles basin, California, between 1972 and 2003, J. Geophys. Res.-Atmos., 113, D23304, doi:10.1029/2008JD009999, 2008.

Novelli, P. C. and Masarie, K. A.: Atmospheric Carbon Monoxide Dry Air Mole Fractions from the NOAA ESRL Carbon Cycle Cooperative Global Air Sampling Network, 1988–2011, Version: 2013-01-28, Path: ftp://ftp.cmdl.noaa.gov/ccg/co/flask/event/, 2012.

Novelli, P., Elkins, J., and Steele, L.: The development and evaluation of a gravimetric reference scale for measurements of atmospheric carbon monoxide, J. Geophys. Res.-Atmos., 96, 13109–13121, 1991.

Pataki, D., Bowling, D., and Ehleringer, J.: Seasonal cycle of carbon dioxide and its isotopic composition in an urban atmosphere: Anthropogenic and biogenic effects, J. Geophys. Res.-Atmos., 108, 4735, doi:10.1029/2003JD003865, 2003.

Press, W. H., Teukolsky, S. A., Vetterling, W. T., and Flannery, B. P.: Numerical Recipes in FORTRAN, 2nd ed., Cambridge Univ. Press, Cambridge, UK, 1992.

Rayner, P. J., Raupach, M. R., Paget, M., Peylin, P., and Koffi, E.: A new global gridded data set of CO_2 emissions from fossil fuel combustion: Methodology and evaluation, J Geophys. Res.-Atmos., 115, D19306, doi:10.1029/2009JD013439, 2010.

Reid, K. and Steyn, D.: Diurnal variations of boundary-layer carbon dioxide in a coastal city – observations and comparison with model results, Atmos. Environ., 31, 3101–3114, 1997.

Rice, A. and Bostrom, G.: Measurements of carbon dioxide in an Oregon metropolitan region, Atmos. Environ., 45, 1138–1144, doi:10.1016/j.atmosenv.2010.11.026, 2010.

Rigby, M., Toumi, R., Fisher, R., Lowry, D., and Nisbet, E. G.: First continuous measurements of CO_2 mixing ratio in central London using a compact diffusion probe, Atmos. Environ., 42, 8943–8953, doi:10.1016/j.atmosenv.2008.06.040, 2008.

Schäfer, K., Emeis, S. M., Rauch, A., and Vogt, C.: Proceedings of SPIE, in Remote Sensing of Clouds and the Atmosphere IX, 5571, 248–259, SPIE. 2004.

Schuh, A. E., Lauvaux, T., West, T. O., Denning, A. S., Davis, K. J., Miles, N., Richardson, S., Uliasz, M., Lokupitiya, E., Cooley, D., Andrews, A., and Ogle, S.: Evaluating atmospheric CO_2 inversions at multiple scales over a highly-inventoried agricultural landscape, Glob. Change Biol., 19, 1424–1439, doi:10.1111/gcb.12141, 2013.

Southon, J. and Santos, G.: Ion source development at KCCAMS, University of California, Irvine, Radiocarbon, 46, 33–39, 2004.

Southon, J. and Santos, G. M.: Life with MC-SNICS. Part II: Further ion source development at the Keck carbon cycle AMS facility, Nucl. Instrum. Meth. B, 259, 88–93, 2007.

Taylor, B. N. and Kuyatt, C. E.: Guidelines for Evaluating and Expressing the Uncertainty of NIST Measurement Results, NIST Technical Note 1297, 1–25, 1996.

Turnbull, J., Miller, J., Lehman, S., Tans, P., Sparks, R., and Southon, J.: Comparison of $^{14}CO_2$, CO, and SF_6 as tracers for recently added fossil fuel CO_2 in the atmosphere and implications for biological CO_2 exchange, Geophys. Res. Lett., 33, L01817, doi:10.1029/2005GL024213, 2006.

Turnbull, J. C., Karion, A., Fischer, M. L., Faloona, I., Guilderson, T., Lehman, S. J., Miller, B. R., Miller, J. B., Montzka, S., Sherwood, T., Saripalli, S., Sweeney, C., and Tans, P. P.: Assessment of fossil fuel carbon dioxide and other anthropogenic trace gas emissions from airborne measurements over Sacramento, California in spring 2009, Atmos. Chem. Phys., 11, 705–721, doi:10.5194/acp-11-705-2011, 2011.

Ulrickson, B. L. and Mass, C. F.: Numerical investigation of mesoscale circulations over the Los Angeles basin. 1. A verification study, Mon. Weather Rev., 118, 2138–2161, 1990.

US Standard Atmosphere: US Government Printing Office, 1976.

van der Kamp, D. and McKendry, I.: Diurnal and seasonal trends in convective mixed-layer heights estimated from two years of continuous ceilometer observations in Vancouver, BC, Bound.-Lay. Meteorol., 137, 459–475, doi:10.1007/s10546-010-9535-7, 2010.

Vogel, F. R., Hammer, S., Steinhof, A., Kromer, B., and Levin, I.: Implication of weekly and diurnal ^{14}C calibration on hourly estimates of CO-based fossil fuel CO_2 at a moderately polluted site in southwestern Germany, Tellus B, 62, 512–520, doi:10.1111/j.1600-0889.2010.00477.x, 2010.

Wallace, J. M. and Hobbs, P. V.: Atmospheric Science: An Introductory Study, 1977th ed. Academic Press, Inc., Orlando, FL, 1977.

Wunch, D., Wennberg, P. O., Toon, G. C., Keppel-Aleks, G., and Yavin, Y. G.: Emissions of greenhouse gases from a North American megacity, Geophys. Res. Lett., 36, L15810, doi:10.1029/2009GL039825, 2009.

Wunch, D., Toon, G. C., Blavier, J. F. L., Washenfelder, R. A., Notholt, J., Connor, B. J., Griffith, D. W. T., Sherlock, V., and Wennberg, P. O.: The Total Carbon Column Observing Network, Philos. T. Roy. Soc. A, 369, 2087–2112, doi:10.1098/rsta.2010.0240, 2011.

Xu, X., Trumbore, S. E., Zheng, S., Southon, J. R., McDuffee, K. E., Luttgen, M., and Liu, J. C.: Modifying a sealed tube zinc reduction method for preparation of AMS graphite targets: Reducing background and attaining high precision, Nucl. Instrum. Meth. B., 259, 320–329, 2007.

Zhao, C., Andrews, A. E., Bianco, L., Eluszkiewicz, J., Hirsch, A., MacDonald, C., Nehrkorn, T., and Fischer, M. L.: Atmospheric inverse estimates of methane emissions from Central California, J. Geophys. Res.-Atmos., 114, D16302, doi:10.1029/2008JD011671, 2009.